Int. J. Electrochem. Sci., 6 **(2011)** 63 - 77

International Journal of
ELECTROCHEMICAL
SCIENCE
www.electrochemsci.org

On the Hydrogen Evolution Reaction at Nickel-Coated Carbon Fibre in 30 wt. % KOH Solution

Boguslaw Pierozynski

Department of Chemistry, Faculty of Environmental Management and Agriculture, University of Warmia and Mazury in Olsztyn, Plac Lodzki 4, 10-957 Olsztyn, Poland
E-mail: bogpierozynski@yahoo.ca

Received: 11 November 2010 / *Accepted:* 1 December 2010 / *Published:* 1 January 2011

The present paper reports an electrochemical study of hydrogen evolution reaction (HER), at commercially available (Toho-Tenax) nickel-coated carbon fibre (NiCCF) material, in 30 wt.% KOH solution. Kinetics of the hydrogen evolution reaction at NiCCF were studied for prolonged time, over the temperature range 22-60 ^{o}C, where the kinetic parameters were derived by means of a.c. impedance spectroscopy for the cathodic overpotential range: -100 to -500 mV/RHE. The effects of cathode deactivation (the result of reversible formation of nickel hydride species) upon continuous electrolysis and its reactivation by dissolved molybdenum (introduced to solution in the form of sodium molybdate) have also been investigated.

Keywords: Nickel-coated carbon fibre; NiCCF; HER; cathode deactivation; molybdenum species.

1. INTRODUCTION

The hydrogen evolution reaction (HER) has extensively been studied on noble metal catalysts, such as polycrystalline and single-crystal surfaces of Pt [1-5] (including ammonia electrolysis for H_2 production, carried-out on Pt [6] and bimetallic (Pt-Ru and Pt-Ir) [7] electrode composites), as well as on other metals and their alloys (e.g. on Ni [8-11], Co [12], Pb [13], Zn-Ni [14], Ni-P [15, 16], Ni-Mo [17], monel® [18] and Ni-Mo-Fe/Ni-Mo-Fe-Co-S [19, 20]).

In short, the HER leads to the formation of bulk H_2 species and proceeds at potentials negative to the H_2 reversible potential. In alkaline media (or for solutions of pH>5), the HER mechanism at metal (Me) electrode is based on a 2-step reaction that involves an adsorbed H intermediate (where H_2O is the proton source), as shown in equations 1-3 below [1, 21]:

$$H_2O + e^- + Me \rightarrow MeH_{ads} + OH^- \quad (Volmer\ electrochemical\ discharge\ step) \quad (1)$$

$$MeH_{ads} + H_2O + e^- \rightarrow H_2 \uparrow + OH^- + Me \quad (Heyrovsky\ electrochemical\ desorption\ step) \quad (2)$$

$$2MeH_{ads} \rightarrow H_2 \uparrow + 2Me \quad (Tafel\ catalytic\ recombination\ step) \quad (3)$$

Commercially available, Toho-Tenax nickel-coated carbon fibre composite [22] is made by electrodeposition of an ultra-thin layer of Ni (*ca*. 0.3-0.5 μm and about 45 wt.% Ni in the composite) onto the surface of 12K (12,000-filament, 7 μm diameter each), PAN-based carbon fibre tow. A sample of Toho-Tenax NiCCF is shown in SEM micrograph images of Figs. 1a and 1b, below.

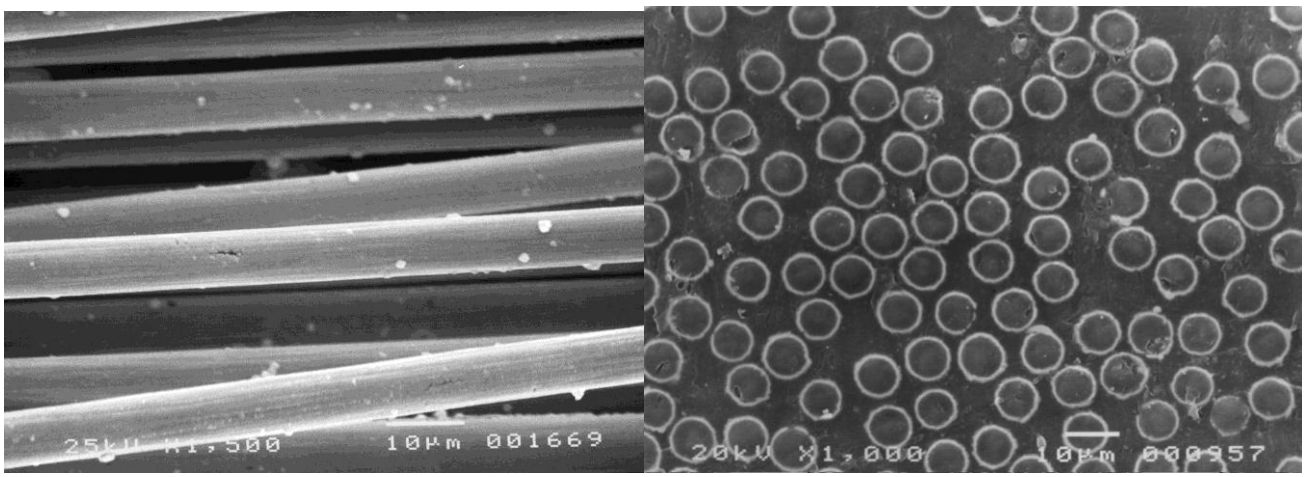

a) **b)**

Figure 1. a) SEM micrograph picture of Toho-Tenax electrodeposited 12K50 NiCCF sample (*ca*. 45 wt.% Ni), taken at 1,500 magnification (powder XRD-calculated Ni grain size for this material came on average to *ca*. 25 nm [50]). b) Cross-sectional sample view, taken at 1,000 magnification.

It can be observed there that the nickel deposit is quite homogeneous throughout the tow (especially evidenced in the cross-sectional view shown in Fig. 1b). NiCCF tow could potentially offer an attractive, large surface-area catalyst material for the process of cathodic evolution of hydrogen. This is because its properties (e.g. electrochemically active surface area, presence of other catalytic co-deposits) can extensively be modified during the processes of carbon fibre pre-treatment and/or Ni deposition. Most importantly, such material could possibly be used to produce large area, *woven* cathodes for the generation of H_2 in commercial electrolysers.

However, it is well-known [9, 10, 23-25] that catalytic metal surfaces (e.g. Ni and Co) undergo progressive deactivation towards the HER upon continuous alkaline water electrolysis. The above is usually revealed in significant increase of overpotential in time, which is attributed to the reversible formation of nickel-hydride species. Such-deactivated cathodes could then become successfully reactivated through the application of specific electrode reactivation procedures, including: *in-situ*

deposition of certain transition metals and periodic interruption of the polarizing current methods [8, 12, 26-33].

This work presents a comprehensive study of the HER on single-tow, Toho-Tenax NiCCF electrodes, carried-out in 30 wt.% KOH solution (similar to that used in commercially-run electrolysers). The electrochemical behaviour of NiCCF tow materials towards the HER has previously been studied in dilute alkaline and acidic media (NaOH and H_2SO_4) by Daftsis et al. [34] and by Pierozynski, and Smoczynski in Ref. 35. In addition, some preliminary findings on this process in 30 wt.% KOH solution have recently been reported by Pierozynski in Ref. 36.

2. EXPERIMENTAL

2.1. Solutions and chemical reagents

A Direct-Q3 UV ultra-pure water purification system from Millipore was used to provide high-purity water (18.2 MΩ cm resistivity) for preparation of 30 wt.% KOH solution (made up from high purity KOH pellets; POCH, Polish Chemical Compounds, p.a.) and for all rinsing purposes. Sodium molybdate, Na_2MoO_4 (99% Na_2MoO_4 x 2 H_2O, Aldrich) was used as the NiCCF cathode *in-situ* re-activation agent, at concentrations about $6.8x10^{-3}$ M. Atmospheric oxygen was removed from solutions before each experiment by bubbling with high-purity Ar (Eurogas, grade 5.0).

2.2. Electrochemical cell, electrodes and experimental methodology

An HDPE made electrochemical cell was used during the course of this work. The cell comprised three electrodes: a nickel-coated carbon fibre working electrode (WE) in a central part, a reversible Pd hydrogen electrode (RHE) as reference and a Pt counter electrode (CE), placed in a separate compartment. The palladium RHE was made of a coiled Pd wire (0.5 mm diameter, 99.9% purity, Aldrich) and sealed in soft glass. Before its use, this electrode was cleaned in hot sulphuric acid, followed by cathodic charging with hydrogen in 0.5 M H_2SO_4, until H_2 bubbles in the electrolyte were clearly observed. The stability of the Pd reference electrode was occasionally checked by recording its potential shift in time, in 30 wt.% KOH solution. No significant potential shift was observed for such prepared Pd reversible hydrogen electrode, up to 120 hours (at room temperature) from its initial H charging. Thus, all the potentials throughout this work are given on the RHE scale. A counter electrode was made of a coiled Pt wire (1.0 mm diameter, 99.9998% purity, Johnson Matthey, Inc.). Prior to its use, the counter electrode was cleaned in hot sulphuric acid.

15 cm long pieces of Toho-Tenax fibre (previously de-sized in acetone in order to remove a protective epoxy resin coating) were used to prepare each NiCCF tow electrode. Prior to conducting the HER experiments, each working electrode (with geometrical surface area of *ca*. 70 cm^2) was activated in 0.5 M H_2SO_4 by cathodic polarization at the current-density of 1 mA cm^{-2} for 900 s, in order to remove any spontaneously formed oxide film and to obtain a reproducible electrode surface.

A.c. impedance spectroscopy and several d.c. electrochemical techniques, including: cyclic voltammetry, galvanostatic and potentiostatic polarizations were employed during the course of this

work. All measurements were conducted by means of the *Solartron* 12608W Full Electrochemical System, consisting of 1260 frequency response analyzer (FRA) and 1287 electrochemical interface (EI). Both galvanostatically and potentiostatically-controlled cathodic polarisations were conducted in the hydrogen evolution region, at the NiCCF electrode surfaces. The selected sweep-rate for cyclic voltammetry experiments was 50 mV s^{-1}.

For impedance measurements, the generator provided an output signal of known amplitude (5 mV) and the frequency range was typically swept between $1.0x10^{5}$ and $0.5x10^{-1}$ Hz. The instruments were controlled by *ZPlot 2.9* or *Corrware 2.9* software for Windows (Scribner Associates, Inc.). Presented impedance results were obtained through selection and analysis of representative series of experimental data. Typically, 2-3 impedance measurements were carried-out at each potential value. Reproducibility of such- obtained results was usually below 10% from one electrode to another. Data analysis was performed with *ZView 2.9* software package, where the impedance spectra were fitted by means of a complex, non-linear, least-squares immitance fitting program, *LEVM 6* (written by J.R. Macdonald in Ref. 37).

The temperature-dependent experiments were conducted by means of a typical thermostatic bath (LWC 1500 type bath, Poland), over the temperature range: 22-60 ^{o}C.

3. RESULTS AND DISCUSSION

3.1. Galvanostatic HER experiments: in-situ reactivation of NiCCF cathodes by dissolved Mo species

Figs. 2a and 2b below present the time-dependent HER behaviour of Toho-Tenax 12K50 NiCCF composite cathodes, when two different current-densities (0.7 and 7.0 mA cm^{-2}: based on the calculated geometrical surface area of electrodes) were applied. It can be seen there that practically continuous (including short breaks for conducting series of a.c. impedance measurements) cathodic polarization of the NiCCF electrode leads to a substantial increase of the recorded overpotential in time (*ca*. 30 mV after 75 hours of cathodic H_2 evolution carried-out at 0.7 mA cm^{-2}, and nearly 100 mV after 20 hours of conducting HER at the current-density of 7.0 mA cm^{-2}). The above behaviour is related to the well-known cathode deactivation effect (see e.g. Refs. 25, 30 and 31), which can be ascribed to the progressive absorption of hydrogen (as Ni hydrides) into the metal lattice (equations 4 and 5 below).

$$NiH_{ads} + Ni_{subsurf} \rightarrow NiH_{abs/subsurf} + Ni_{surf} \text{ (H absorption in the subsurface layer)} \quad (4)$$

$$NiH_{abs/subsurf} \rightarrow NiH_{abs/bulk} \text{ (H diffusion into the bulk of metal)} \quad (5)$$

Introduction of sodium molybdate (at $6.8x10^{-3}$ M) upon 75 hours of cathodic polarization at 0.7 mA cm^{-2} causes an immediate, major jump of cathode overpotential (with severe potential fluctuation though) towards a direction of the electrode recovery. At 120 hours, the NiCCF cathode overpotential reaches the value of *ca*. -120 mV; however, a significant potential fluctuation is still present (see Fig. 2a again).

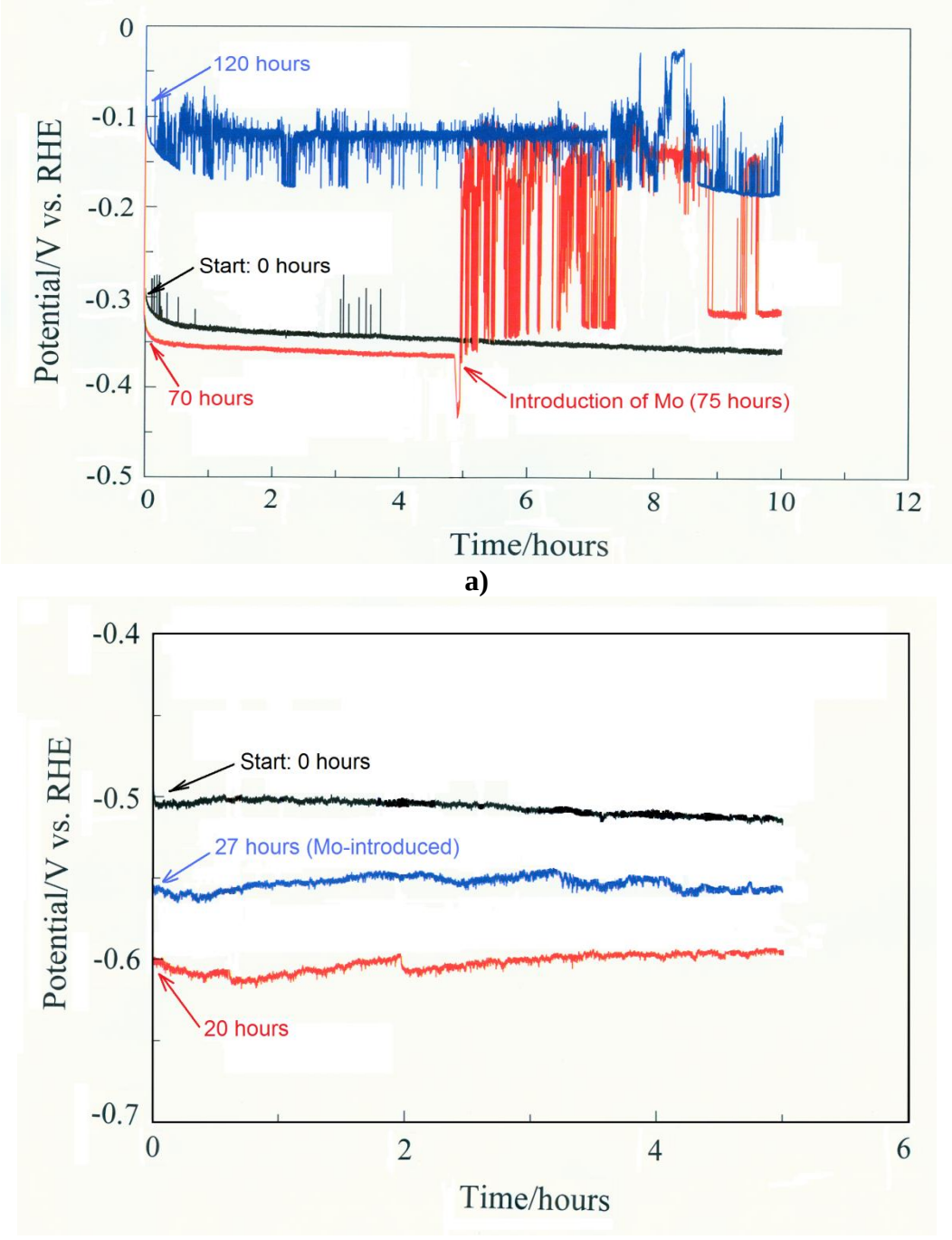

Figure 2. a) Potential (IR-corrected) vs. time response for galvanostatically carried-out HER on Toho-Tenax 12K50 NiCCF electrode (at cathodic current-density, j_c= 0.7 mA cm^{-2}) in 30 wt.% KOH solution, at *ca*. 30 ^{o}C. b) As in (a), but for the experiments carried-out at current-density of 7.0 mA cm^{-2}.

In other words, introduction of Mo species not only causes full electrode reactivation, but also significantly modifies the NiCCF cathode to the state that is about 200 mV lower in overpotential, as compared to an initial electrode condition. On the other hand, the corresponding effect of Mo addition

for the "high" current-density (7.0 mA cm^{-2}) HER run is much less significant. Here, introduction of Mo causes an immediate recovery of the cathode by 40-50 mV, but without any distinct potential fluctuation (Fig. 2b). However, this effect does *not* become further enhanced, as the cathodic polarization continues.

The a.c. impedance characterization of the HER at Toho-Tenax NiCCF electrode in contact with 30 wt.% KOH is presented in Fig. 3 below.

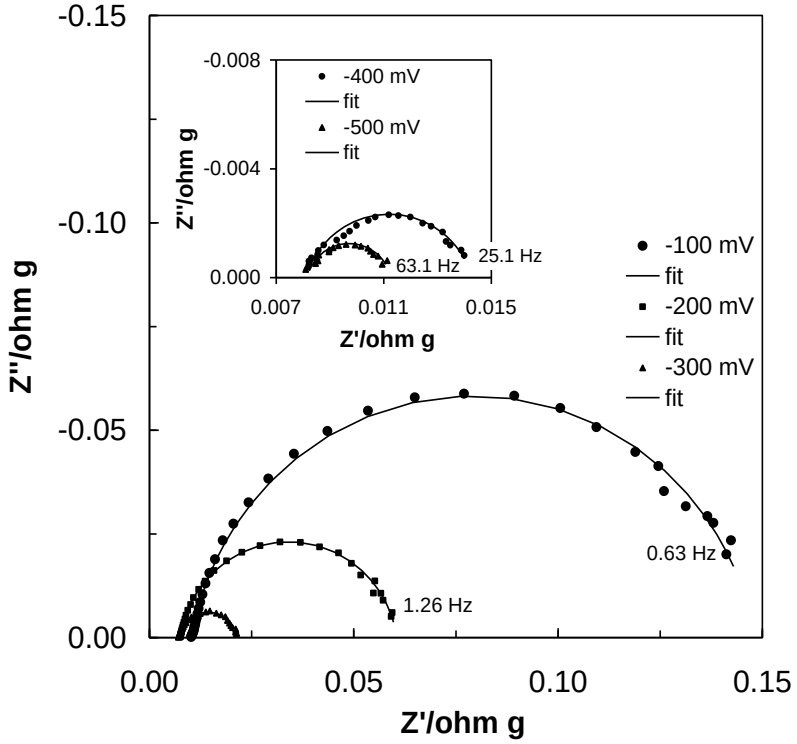

Figure 3. Complex-plane impedance plots for Toho-Tenax 12K50 NiCCF tow electrode in contact with 30 wt.% KOH solution, recorded at room temperature on a fresh fibre electrode, for overpotentials: -100 through -500 mV (vs. RHE). The solid lines correspond to representation of the data according to the equivalent circuit shown in Fig. 4.

Here, a single-step charge-transfer reaction system was considered, where the electrode exhibited single, "depressed" semicircles at all studied potentials, in the explored frequency range. The presence of a second, high-frequency semicircle (as often observed for porous materials in alkaline media [38-44]) for overpotentials greater than -200 mV was always ambiguous in this work. Moreover, when discernible, the corresponding high-frequency semicircle-derived resistance would only count to *ca*. 0.5-2.0% of that related to the main semicircle (R_{ct}- charge-transfer resistance parameter). Thus, all kinetic parameters were derived from the analysis of the large (intermediate/low frequency) semicircle by means of an equivalent circuit model presented in Fig. 4.

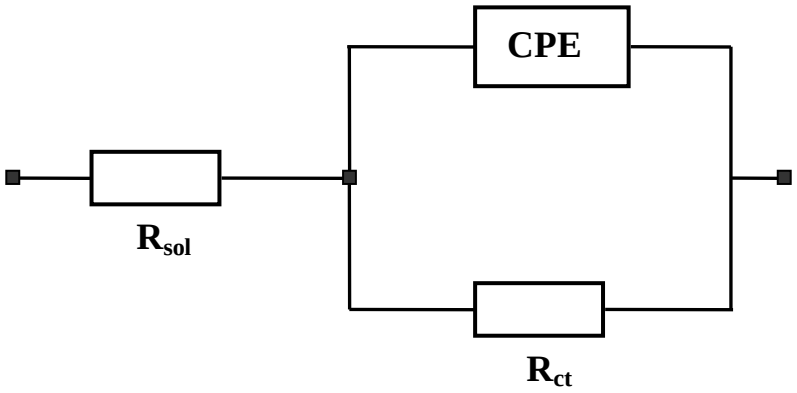

Figure 4. An equivalent circuit model used for fitting the impedance data for Toho-Tenax 12K50 NiCCF tow electrodes, obtained in 30 wt.% KOH solution. The circuit exhibits a Faradaic charge-transfer resistance (R_{ct}) in a parallel combination with the double-layer capacitance (C_{dl}) [represented by the constant phase element (CPE) for distributed capacitance], jointly in series with an uncompensated solution resistance (R_{sol}) parameter (an average, impedance-derived value of R_{Sol} oscillated around 0.012-0.015 Ω g).

Table 1 below presents variation of overpotential-dependent (-100 to -500 mV/RHE) Faradaic reaction resistance, R_{ct} parameter for the Toho-Tenax fibre electrodes in contact with 30 wt.% KOH solution with time of electrolysis, given for two series of galvanostatically performed HER experiments. From the analysis of the R_{ct} data in Table 1 it can be concluded that initially for both applied current-densities (0.7 and 7.0 mA cm^{-2}) the NiCCF cathodes undergo progressive deactivation. Thus, at -100 mV a relative increase of the R_{ct} parameter is *ca*. 7.1 and 11.8 after 30 hours (at j_c= 0.7 mA cm^{-2}) and after 25 hours (at j_c= 7.0 mA cm^{-2}) of cathodic H_2 generation, respectively. Introduction of Mo species causes a substantial reduction of the charge-transfer resistance parameter. Hence, the final R_{ct} (at the potential of -100 mV) values of 0.028 and 0.458 Ω g were recorded at 120 hours (for j_c= 0.7 mA cm^{-2}) and at 57 hours (for j_c= 7.0 mA cm^{-2}) of cathodic H_2 evolution, giving the R_{ct} ratios (final-to-initial) of 0.2 and 3.6, correspondingly. These results (also valid for other overpotentials, see Table 1 again) are *in-line* with those reported in Figs. 2a and 2b, where the final electrode overpotential for the "low" current-density HER run is significantly lower (by about 200 mV) than its initial value. On the other hand, only partial electrode recovery was achieved for the "high" current-density HER trial (refer to Fig. 2b). Interestingly, it can also be observed in Table 1 (especially for the "low" current-density HER run) that the R_{ct} parameter (following the peak value) starts declining (the electrode commences its recovery) even before introduction of sodium molybdate into the solution takes place. The above phenomenon will be discussed later in this paragraph in more detail.

Furthermore, a plot of –log R_{ct} vs. overpotential (η) showed a fairly good linear relationship for all examined data series in Table 1, over the studied potential range. Examples of the –log R_{ct}= f(η) relationship for the two series of HER runs [LC: *low current*-density (0.7 mA cm^{-2}) and HC: *high current*-density (7.0 mA cm^{-2})] are presented in Fig. 5 below. These results are in agreement with the kinetically-controlled process that proceeds via the Volmer-Heyrovski route (equations 1 and 2 above) over the studied overpotential range [38, 44-46]. Moreover, based on the well-known Butler-Volmer

equation and by utilizing the relation between the exchange current-density (j_0) and the R_{ct} parameter for $\eta \longrightarrow 0$ (equation 6):

$$j_0 = \frac{RT}{zFR_{ct}} \qquad (6)$$

the exchange current-density parameter for the HER on examined data series was calculated.

Table 1. Variation of the charge-transfer resistance (R_{ct}) parameter (±4%) with time for galvanostatically carried-out HER (at *ca*. 30 °C and current-densities of 0.7 and 7.0 mA cm^{-2}) on Toho-Tenax 12K50 NiCCF tow electrodes in 30 wt.% KOH solution, obtained by fitting the equivalent circuit (Fig. 4) to the experimentally obtained impedance data, for overpotentials: -100 through -500 mV vs. RHE.

E/ mV	Galvanostatic HER (j_c= 0.7 mA cm^{-2})							
	R_{ct}/ Ω g							
	Start	20 h	30 h	40 h	60 h	80 h$^{(*)}$	100 h	120 h
-100	0.138	0.834	0.975	0.328	0.454	0.113	0.161	0.028
-200	0.052	0.412	0.422	0.253	0.268	0.110	0.013	0.024
-300	0.014	0.047	0.045	0.036	0.039	0.031	0.011	0.011
-400	0.006	0.012	0.011	0.010	0.011	0.010	0.007	0.006
-500	0.003	0.005	0.005	0.005	0.006	0.006	0.004	0.002
E/ mV	Galvanostatic HER (j_c= 7.0 mA cm^{-2})							
	R_{ct}/ Ω g							
	Start	10 h	20 h	25 h	32 h$^{(**)}$	42 h	52 h	57 h
-100	0.127	1.651	1.397	1.498	0.325	0.455	0.383	0.458
-200	0.041	0.345	0.502	0.608	0.153	0.194	0.167	0.184
-300	0.011	0.052	0.103	0.151	0.061	0.083	0.057	0.065
-400	0.004	0.014	0.023	0.034	0.023	0.028	0.029	0.033
-500	0.003	0.005	0.008	0.010	0.009	0.008	0.011	0.012

* Mo was introduced at 75.0 h.
** Mo was introduced at 26.5 h.

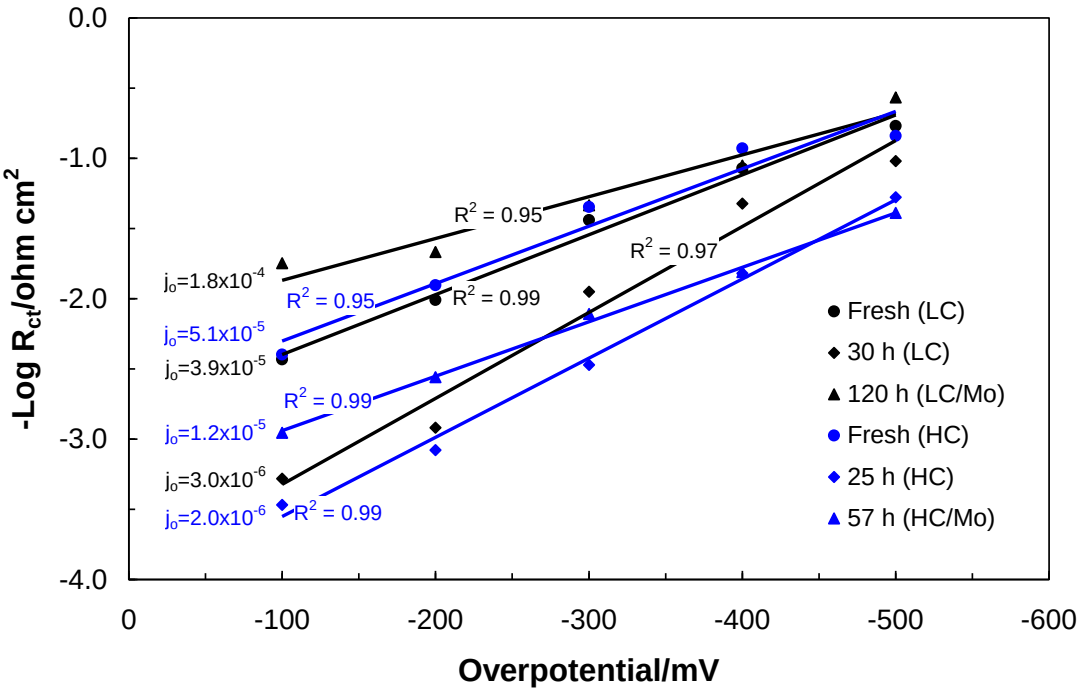

Figure 5. Linear plots of –log R_{ct} vs. overpotential, obtained for the HER performed on Toho-Tenax 12K50 NiCCF tow electrodes in 30 wt.% KOH solution (LC & HC symbols correspond to *low* and *high* current-density galvanostatic HER experiments, recorded at specified time runs). Symbols represent experimental results and lines are data fits.

Thus, for the LC HER data series in Fig. 5, j_0 values of $3.9x10^{-5}$, $3.0x10^{-6}$ and $1.8x10^{-4}$ A cm^{-2} were derived for a fresh electrode, after 30 hours and after 120 hours (with dissolved Mo present) of cathodic H_2 evolution, correspondingly. Thus, the highest value of the exchange current-density was recorded for a Mo-reactivated NiCCF cathode (*ca*. 4.6 and 60.0 times as high as the j_0 values recorded for the fresh and a deactivated cathode, respectively). Similar results are presented in Fig. 5 for the HC HER data series; however, the recorded j_0 value for the Mo-reactivated cathode ($1.2x10^{-5}$ A cm^{-2}) is still significantly smaller than that originally recorded on the fresh NiCCF electrode ($5.1x10^{-5}$ A cm^{-2}). All calculated in this work exchange current-densities are within the range that is commonly quoted for Ni in literature [30, 32, 38, 44-46].

On the other hand, the double-layer capacitance parameter, C_{dl} (represented by the constant phase element: CPE for distributed capacitance [47, 48] in Fig. 4) did tend to substantially increase (based on the C_{dl} recorded at the potential of -100 mV) in time upon the HER experiments, carried-out both at LC and HC galvanostatic conditions (see Fig. 6 below). Thus, the recorded C_{dl} values for fresh NiCCF cathodes came to $149x10^3$ (LC) and $223x10^3$ μF g^{-1} $s^{\varphi-1}$ (HC), which accounted for *ca*. 75.8 and 113.5 μF cm^{-2} $s^{\varphi-1}$ (with respect to their geometrical surface area), respectively (compare with the corresponding C_{dl} values reported for NiCCF in Refs. 34 and 35). However, extended cathodic polarizations almost immediately led to a dramatic increase of the double-layer capacitance, reaching 442.5 (at 120 hours) and 531.6 μF cm^{-2} $s^{\varphi-1}$ (at 57 hours) for the LC and the HC HER runs, respectively. These values correspond to an increase by about 5.8 or 4.7 times of the C_{dl} parameter for the respective HER series. Simultaneously, the dimensionless φ parameter (φ determines the constant

phase angle in the complex-plane plot and $0 \leq \varphi \leq 1$) of the CPE circuit (Fig. 4) varied between 0.83-0.90 (LC HER series) and 0.83-0.92 for the HC HER run (see Fig. 6 again).

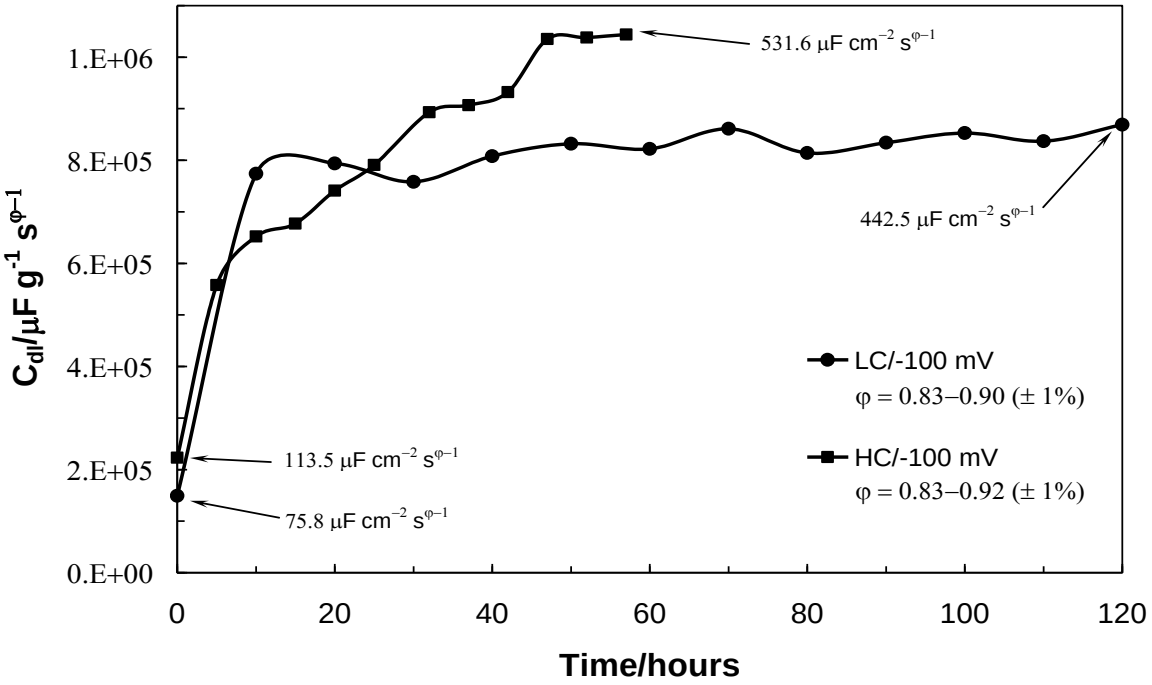

Figure 6. Variation of the double-layer capacitance (C_{dl}) parameter (with an error less than ±3%) with time for the HER carried-out on Toho-Tenax NiCCF tow electrodes in 30 wt.% KOH solution, obtained by fitting the equivalent circuit shown in Fig. 4 to the experimentally obtained impedance data, at overpotential of -100 mV vs. RHE (other details as in Fig. 5).

In summary, a substantial increase in the double-layer capacitance along with significant reduction of the charge-transfer resistance parameter (increase of the exchange current-density) upon the cathodic evolution of hydrogen with dissolved Mo species would imply a considerable surface roughening effect. It is strongly believed that this effect is primarily related to substantial Mo electrodeposition on the NiCCF surface, which leads to a significant increase of an electrochemically active surface of the NiCCF composite cathodes. The above gets some support from the fact that an appreciable electrode recovery (especially for the LC HER run) can already be observed prior to introduction of Mo into the solution (see Table 1 again). This "preliminary" cathode recovery can be attributed to simultaneous (*in-line* with the HER) electrodeposition of metallic impurities from the electrolyte (e.g. compare with similar findings in Refs. 12 and 30).

3.2. Temperature-dependent HER studies

Fig. 7 presents $-\log R_{ct}$ vs. T^{-1} (Arrhenius-type) plots, constructed based on the $R_{ct}=f(T)$ a.c. impedance results, presented for the overpotential range: -100 to -500 mV (RHE) in Table 2 below. From the overpotential-dependent slopes of lines shown in Fig. 7, the corresponding, experimental,

electrochemical energies of activation E* [kJ mol^{-1}] for the HER at the Toho-Tenax NiCCF cathode were also derived and presented in Table 2.

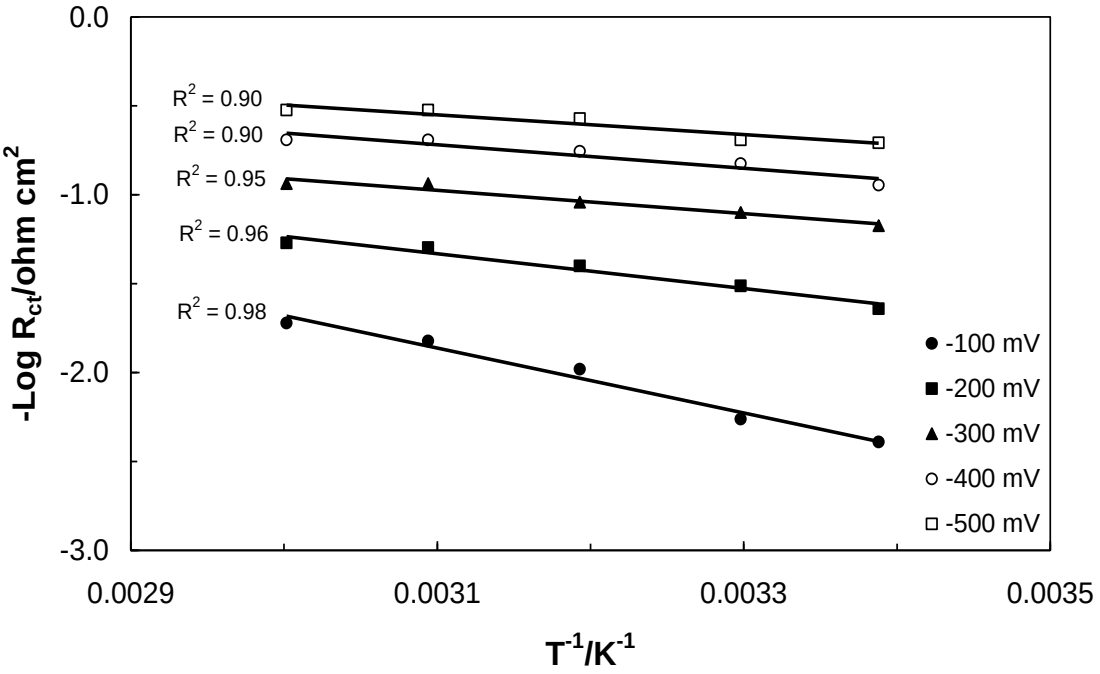

Figure 7. Linear plots of –log R_{ct} vs. T^{-1} for the HER performed on Toho-Tenax 12K50 NiCCF tow electrode in 30 wt.% KOH solution, at the stated overpotential values.

Table 2. Variation of the charge-transfer resistance (R_{ct}) parameter (±4%) with temperature for the HER carried-out on Toho-Tenax 12K50 NiCCF tow electrode in 30 wt.% KOH solution, obtained by fitting the equivalent circuit (Fig. 4) to the experimentally obtained impedance data, for overpotentials: -100 through -500 mV vs. RHE. Experimentally derived, electrochemical activation energies (E*) in function of the applied overpotential.

E/ mV*	R_{ct}/ Ω g					E*/ kJ mol^{-1}
	22 °C	30 °C	40 °C	50 °C	60 °C	
-100	0.1250	0.0932	0.0487	0.0338	0.0268	34.9
-200	0.0223	0.0166	0.0128	0.0101	0.0095	18.8
-300	0.0076	0.0064	0.0056	0.0044	0.0044	12.5
-400	0.0045	0.0034	0.0029	0.0025	0.0025	12.6
-500	0.0026	0.0025	0.0019	0.0017	0.0017	10.6

* An appropriate correction was introduced [51], in order to account for a small, but significant temperature shift of the Pd RHE over the studied temperature range: 22-60 °C.

When such-obtained electrochemical energies of activation were plotted in function of the overpotential (Fig. 8), an ultimate enthalpy potential for the HER on the Toho-Tenax fibre cathode (at -906 mV) was determined [49].

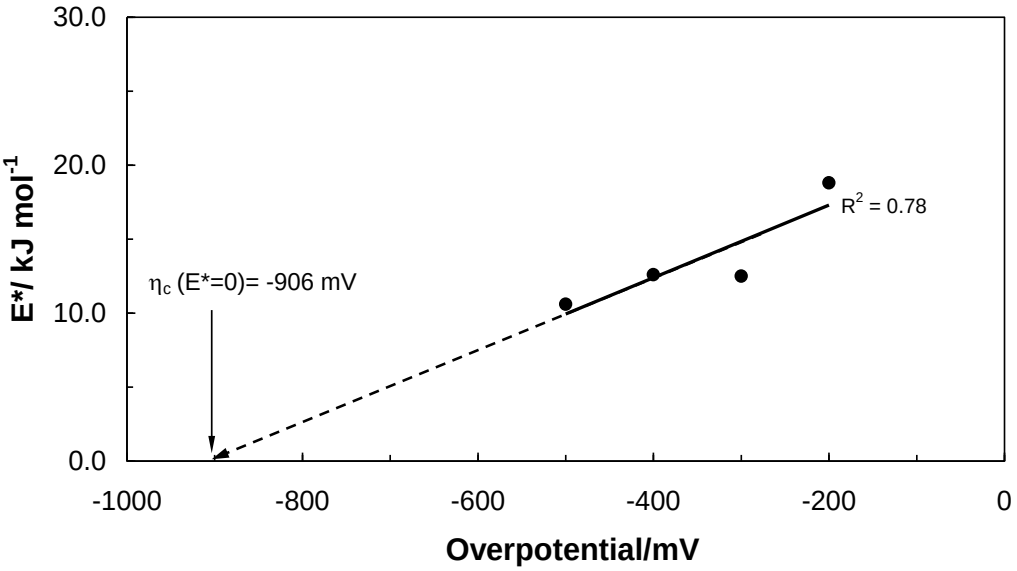

Figure 8. Dependence of experimentally-derived, electrochemical energies of activation (E*) vs. overpotential for the HER carried-out on Toho-Tenax 12K50 NiCCF electrode in 30 wt.% KOH solution (please note that in order to increase the accuracy of the fit, the calculated E* value for -100 mV was eliminated from the plot).

In other words, for overpotentials below *ca*. 900 mV, the HER rate on the NiCCF cathode should no longer be dependent on the applied electrode potential.

3.3. Cyclic voltammetry, in-situ reactivation of NiCCF cathodes

Once the Toho-Tenax NiCCF electrodes had been deactivated (through potentiostatically-controlled HER, with the cathode set at -0.5 V/RHE for one hour), they were then subjected to a cyclic voltammetry treatment, involving CV scanning over the potential range 0.0 to 1.0 V (see Fig. 9). An initial part of the cyclic voltammetric profile shown in Fig. 9 reveals an anodic oxidation peak at the potential range *ca*. 0.1 through 0.5 V. Then, this peak disappears as the NiCCF cathode is continuously cycled within the potential range that is positive to the H_2 reversible potential. The above behaviour is reminiscent of the process of subsurface nickel hydride [23-25] formation upon the hydrogen evolution reaction (refer to equations 4 and 5 above), which is then followed by anodic hydrogen oxidation reaction (HOR), over the potential range *ca*. 0.0-0.5 V.

The above becomes confirmed through evaluations of the charge-transfer resistance parameter values (see Table 3 below), recorded in a sequence for: a) fresh, b) deactivated and c) CV-reactivated Toho-Tenax NiCCF electrode. Thus, the R_{ct} values calculated for a deactivated cathode are *ca*. 5.5,

2.5, 1.5 and 1.7 times as high as those recorded for a fresh one, at: -100, -200, -300 and -400 mV/RHE, respectively.

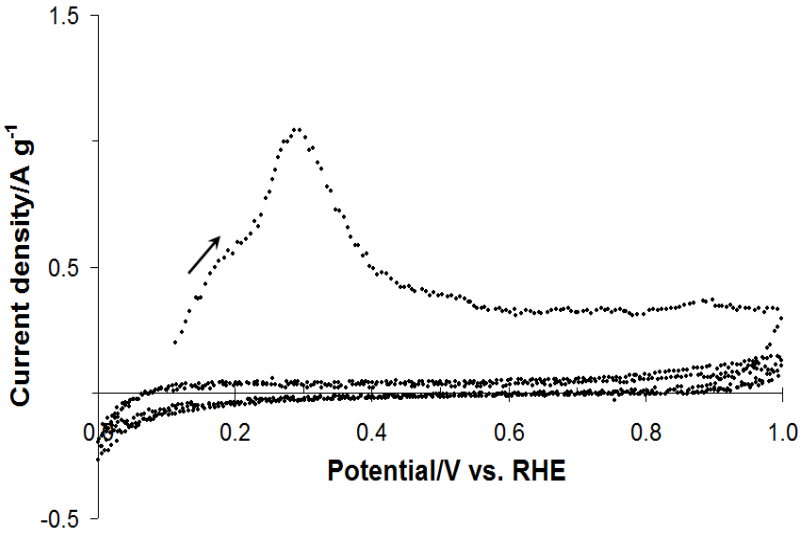

Figure 9. Cyclic voltammetry reactivation of Toho-Tenax 12K50 NiCCF electrode in 30 wt.% KOH solution, recorded at a sweep rate of 50 mV s^{-1} over the potential range 0.0-1.0 V/RHE [36].

Table 3. Variation of the charge-transfer resistance (R_{ct}) parameter (±2%) for the HER carried-out on: fresh, deactivated and CV-reactivated Toho-Tenax NiCCF 12K50 tow electrode in 30 wt.% KOH solution, obtained by fitting the equivalent circuit (Fig. 4) to the experimentally obtained impedance data (at room temperature), for selected overpotential values.

E/mV	R_{ct}/Ω g (fresh)	R_{ct}/Ω g (deactivated)	R_{ct}/Ω g (CV-reactivated)
-100	0.110	0.610	0.096
-200	0.042	0.105	0.041
-300	0.011	0.017	0.011
-400	0.003	0.005	0.002

On the other hand, the CV treatment leads practically to a complete electrochemical reactivation of the electrode, with the set of the charge-transfer resistance values on the order of those characteristic of the fresh electrode surface (compare the CV-reactivated values of the R_{ct} parameter with those of the fresh electrode in Table 3).

4. CONCLUSIONS

Extended cathodic polarizations of Toho-Tenax 12K50 NiCCF composite cathodes, performed in contact with 30 wt.% KOH solution caused substantial electrode deactivation (strongly-dependent on the applied current-density), being the result of the reversible formation of nickel hydride species. Introduction of dissolved Mo species to the KOH electrolyte (following cathode deactivation) resulted in almost immediate and effective electrode reactivation. The above can primarily be attributed to the substantial increase of electrochemically active surface area of the NiCCF cathode brought about by the presence of surface-electrodeposited Mo species (in addition to the possible effect of partial decomposition of nickel hydride layer). Another convenient way to carry-out *in-situ* reactivation of the NiCCF cathode involves cyclic voltammetry sweep towards hydrogen oxidation, conducted over the potential range 0.1 to 0.5 V (RHE).

Finally, Toho-Tenax NiCCF offers an attractive, large surface-area material for the process of cathodic evolution of hydrogen. It has been proven in this work that a small (2.5 cm long) piece of this material (having a geometrical surface area of *ca*. 70 cm^2) managed to effectively generate hydrogen for 120 hours, with an imposed cathodic current of -50 mA [the above translates to 2 A for a 1 m long (*ca*. 0.28 m^2) piece of fibre for the LC case]. Therefore, it seems important that current work be extended to a technical scale alkaline water electrolysis setup, where the large surface area NiCCF cathode material (likely in the form of woven entities) would be subjected to the HER testing at cathodic currents as high as 100 A or more. Such an electrolyser could be operated on a fairly continuous basis, where reactivation of the cathode(s) would be realized *in-situ* (e.g. via introduction of Mo species) or by periodical cyclic voltammetry HOR treatments.

References

1. J. Barber, S. Morin, B.E. Conway, *J. Electroanal. Chem*., 446, (1998), 125.
2. J.H. Barber, B.E. Conway, *J. Electroanal. Chem*., 461, (1999), 80.
3. B.E. Conway, B.V. Tilak, *Electrochim. Acta*, 47, (2002), 3571.
4. A.C.D. Angelo, *Int. J. Hydrogen Energy*, 32, (2007), 542.
5. N.M. Markovic, S.T. Sarraf, H.A. Gasteiger, P.N. Ross, *J. Chem. Soc., Faraday Trans*., 92, (1996), 3719.
6. L. Zhou, Y.F. Cheng, *Int. J. Hydrogen Energy*, 33, (2008), 5897.
7. F. Vitse, M. Cooper, G.G. Botte, *J. Power Sources*, 142, (2005), 18.
8. J.Y. Huot, L. Brossard, *Int. J. Hydrogen Energy*, 12(12), (1987), 821.
9. H.E.G. Rommal, P.J. Moran, *J. Electrochem. Soc*., 135(2), (1988), 343.
10. D.M. Soares, O. Teschke, I. Torriani, *J. Electrochem. Soc*., 139(1), (1992), 98.
11. C. Hitz, A. Lasia, *J. Electroanal. Chem*., 500, (2001), 213.
12. J.Y. Huot, L. Brossard, *J. Appl. Electrochem.*, 18, (1988), 815.
13. Y.M. Wu, W.S. Li, X.M. Long, F.H. Wu, H.Y. Chen, J.H. Yan, C.R. Zhang, *J. Power Sources*, 144, (2005), 338.
14. G. Sheela, M. Pushpavanam, S. Pushpavanam, *Int. J. Hydrogen Energy*, 27, (2002), 627.
15. T. Burchardt, *Int. J. Hydrogen Energy*, 25, (2000), 627.
16. A. Krolikowski, A. Wiecko, *Electrochim. Acta*, 47, (2002), 2065.
17. K. Hashimoto, T. Sasaki, S. Meguro, K. Asami, *Mater. Sci. Eng. A*, 375-377, (2004), 942.
18. J.C. Ganley, *Int. J. Hydrogen Energy*, 34, (2009), 3604.

19. M. Jayalakshmi, W.Y. Kim, K.D. Jung, O.S. Joo, *Int. J. Electrochem. Sci*., 3, (2008), 908.
20. M. Jayalakshmi, I. Puspitasari, K.D. Jung, O.S. Joo, *Int. J. Electrochem. Sci*., 3, (2008), 787.
21. B.E. Conway, B.V. Tilak, *Adv. Catalysis*, 38, (1992), 1.
22. *Tenax®MC HTA A302 Nickiel-coated filament yarn. Material Safety Data Sheet,* http://www.tohotenax-eu.com (2010).
23. L. Vracar, B.E. Conway, *J. Electroanal. Chem*., 277, (1990), 253.
24. M. Bernardini, N. Comisso, G. Davolio, G. Mengoli, *J. Electroanal. Chem*., 442, (1998), 125.
25. R. Juskenas, R. Giraitis, V. Pakstas, *Chemija*, 13(1), (2002), 26.
26. J.Y. Huot, L. Brossard, *Int. J. Hydrogen Energy*, 14(4), (1989), 229.
27. J.Y. Huot, L. Brossard, *Surf. Coat. Tech.*, 34, (1988), 373.
28. H.E.G. Rommal, P.J. Moran, *J. Electrochem. Soc*., 132(2), (1985), 325.
29. R.M. Abouatallah, D.W. Kirk, S.J. Thorpe, J.W. Graydon, *J. Electrochem. Soc.*, 148(9), (2001), E357.
30. R.M. Abouatallah, D.W. Kirk, S.J. Thorpe, J.W. Graydon, *Electrochim. Acta*, 47, (2001), 613.
31. R.M. Abouatallah, D.W. Kirk, J.W. Graydon, *Electrochim. Acta*, 47, (2002), 2483.
32. H. He, H. Liu, F. Liu, K. Zhou, *Surf. Coat. Tech.*, 201, (2006), 958.
33. A.E. Mauer, D.W. Kirk, S.J. Thorpe, *Electrochim. Acta*, 52, (2007), 3505.
34. E. Daftsis, N. Pagalos, A. Jannakoudakis, P. Jannakoudakis, E. Theodoridou, R. Rashkov, M. Loukaytsheva, N. Atanassov, *J. Electrochem. Soc.*, 150(11), (2003), C787.
35. B. Pierozynski, L. Smoczynski, *J. Electrochem. Soc*., 156(9), (2009), B1045.
36. B. Pierozynski, *Environ. Biotech*., 6(1), (2010), 1.
37. J.R. Macdonald, *Impedance Spectroscopy, Emphasizing Solid Materials and Systems*, John Wiley & Sons, Inc., New York, (1987).
38. R.K. Shervedani, A.R. Madram, *Electrochim. Acta*, 53, (2007), 426.
39. A. Lasia in: B.E. Conway, J.O.M. Bockris, R. White, *Modern Aspects of Electrochemistry*, vol. 32, Kluwer, New York, (1999), 143.
40. A. Lasia, *J. Electroanal. Chem*., 500, (2001), 30.
41. B. Losiewicz, A. Budniok, E. Rowinski, E. Lagiewka, A. Lasia, *Int. J. Hydrogen Energy*, 29, (2004), 145.
42. J. Panek, A. Serek, A. Budniok, E. Rowinski, E. Lagiewka, *Int. J. Hydrogen Energy*, 28, (2003), 169.
43. R.K. Shervedani, A. Lasia, *J. Appl. Electrochem*., 29, (1999), 979.
44. N. Krstajic, M. Popovic, B. Grgur, M. Vojnovic, D. Sepa, *J. Electroanal. Chem*., 512, (2001), 16.
45. J.G. Highfield, E. Claude, K. Oguro, *Electrochim. Acta*, 44, (1999), 2805.
46. S. Martinez, M. Metikos-Hukovic, L. Valek, *J. Mol. Cat. A: Chem*., 245, (2006), 114.
47. T. Pajkossy, *J. Electroanal. Chem*., 364, (1994), 111.
48. B.E. Conway, in: E. Barsoukov, J. Ross Macdonald (Eds.), *Impedance Spectroscopy. Theory Experiment and Applications*, Wiley-Interscience, John Wiley & Sons Inc., Hoboken, NJ, Chapter 4.5.3.8, (2005), 494.
49. N. Krstajic, M. Popovic, B. Grgur, M. Vojnovic, D. Sepa, *J. Electroanal. Chem*., 512, (2001), 27.
50. B. Pierozynski, L. Smoczynski, *J. Electrochem. Soc*., 155(8), (2008), C427.
51. A. Prokopowicz, M. Opallo, *Solid State Ionics*, 157, (2003), 209.